Structure and propagation of n-heptane/air premixed flame in low temperature ignition regime

Zhong, Shenghui ; Zhang, Fan ; Jangi, Mehdi; Bai, Xue Song; Yao, Mingfa; Peng, Zhijun

Structure and propagation of n-heptane/air premixed flame in low temperature ignition regime[☆]

Shenghui Zhong[a,b], Fan Zhang[a*], Mehdi Jangi[c], Xue-Song Bai[b], Mingfa Yao[a], Zhijun Peng[a*]

[a] State Key Laboratory of Engines, Tianjin University, 135 Yaguan Rd, Tianjin, China, 300350

[b] Department of Energy Sciences, Lund University, PO Box 118, SE-221 00 Lund, Sweden

[c] Department of Mechanical Engineering, University of Birmingham, B15 2TT Birmingham, United Kingdom

[*]Corresponding author: fanzhang_lund@tju.edu.cn, pengzj@tju.edu.cn.

[☆]The short version of the paper (paper ID #74) was presented at ICAE2019, Aug 12-15, Västerås, Sweden. This paper is a substantial extension of the short version of the conference paper

Highlights

- Premixed n-heptane/air flame in low temperature ignition (LTI) regime is investigated
- In LTI regime heat release zone is broader than in chemically frozen (CF) regime
- Turbulent and laminar burning velocities are higher in LTI regime than in CF regime
- Mechanisms of enhanced burning velocity in LTI regime are proposed
- Differential diffusion is more important in LTI regime than in CF regime

Abstract

This paper presents a large eddy simulation of n-heptane/air turbulent premixed combustion in a reactor assisted turbulent slot (RATS) burner under different preheating conditions. N-heptane/air mixture at an equivalence ratio of 0.6, pressure of 1 atm and temperature of 600, 650 and 700 K is considered to investigate the effect of low temperature chemistry on turbulent burning velocities and flame regimes, including

chemically frozen (CF) regime where the fuel/air mixture inside the burner is chemically frozen, low temperature ignition (LTI) regime where the fuel/air mixture inside the burner undergoes LTI reactions, and transition regime from CF to LTI. The results show that the flame in the LTI regime exhibits the highest turbulent burning velocity. Differential diffusion is found to play an important role in the LTI regime whereas it is less important in the CF regime. To investigate the effect of LTI reactions on the flame, a series of two-dimensional laminar flames are simulated, in which the effect of turbulence on the flames is eliminated. The results show that in the LTI regime, the laminar burning velocity is drastically enhanced and the heat release zone is broadened. Budget term analysis shows that the enhanced rate of production and diffusion towards the preheat zone of the flames and the smaller gradient of reactant mass fraction are the main reasons behind the increased laminar burning velocity in the LTI regime.

Keyword: low temperature ignition, burning velocity, differential diffusion, fuel reactivity, turbulent premixed flame

Abbreviations

CF	Chemically Frozen
DNS	Direct Numerical Simulation
GCI	Gasoline Compression Ignition
HRR	Heat Release Rate
HTI	High Temperature Ignition

IC	Internal Combustion
ICCI	Intelligent Charge Compression Ignition
LES	Large Eddy Simulation
LTI	Low Temperature Ignition
LTR	Low Temperature Reforming
PPC	Partially Premixed Combustion
RATS	Reactor Assisted Turbulent Slot
RCCI	Reactivity Controlled Compression Ignition
ROP	Rate of Production
WSR	Well-Stirred Reactor
0D	Zero-Dimensional
1D	One-Dimensional
2DLF	Two-Dimensional Laminar Flame
3D	Three-Dimensional

1. Introduction

Combustion will be the main energy conversion approach in the transport sector for decades to come [1]. Conventional diesel combustion [2] and advanced combustion concepts in internal combustion (IC) engines, for example, reactivity controlled compression ignition (RCCI) [3], partially premixed combustion (PPC) [4][5], gasoline compression ignition (GCI) [6] and intelligent charge compression ignition (ICCI) [7], are being developed to achieve higher thermal efficiency and lower emissions. Most of the advanced IC engine concepts operate at low temperature with transportation fuels such as gasoline and diesel [8]. Large hydrocarbon fuels generally exhibit two-stage ignition behavior, consisting of a low temperature ignition (LTI) stage and a high

temperature ignition (HTI) stage [9]. The LTI stage becomes rather significant under cold-start conditions in IC engines [10][11]. In addition, LTI has shown to play an important role in cool flame [12][13], plasma assisted combustion [14], engine knock [15], premixed flame propagation [16], spray combustion under IC engine conditions [11][17], and combustion process involved in fuel reforming technology [18][19]. Understanding the underlying physics of the LTI, its coupling with heat and mass transfer and chemical kinetics, and the impact of LTI on turbulent flame structures and burning velocities will contribute significantly to the improvement of engine performance [20].

It is well recognized that turbulent burning velocity (S_T) increases with increasing turbulent intensities due to the increasing flame surface wrinkling in a low-to-medium turbulence intensity range. After the LTI stage, the reactant composition and temperature change, which in turn affects the mixture Lewis number (*Le*) and laminar burning velocity (S_L) [21]. Experiments in a so-called RATS (reactor assisted turbulent slot) burner [16] have been carried out to study the increased S_T following the onset of LTI. The focus was on the changes in high temperature reactivity and the thermo-diffusive properties of the reactant mixture. It was found that the increased S_T in the LTI regime is due to the change of turbulent flow, a decrease of the Lewis number and an increase of S_L [21]. LTI was shown to significantly affect turbulent burning velocity. It was speculated that this is due to the increased reactivity after LTI [21]. By matching the initial conditions to that in the RATS burner, Savard et al. [22] performed a direct

numerical simulation (DNS) of n-heptane/air turbulent premixed flame in an isotropic turbulent flow, and the data were used to evaluate the effect of LTI on S_T in the LTI regime. It was shown that the increase of S_L is a dominant factor in the enhancement of S_T, while turbulence does not affect the relative contribution of the key chemical reactions. The important impact of LTI on the structure and propagation of premixed flames has been observed for other fuels. In a recent detailed numerical study of DME (dimethyl ether) laminar premixed flame at elevated initial temperature, Krisman et al. showed that four different combustion regimes could be identified, based on the ignition time and residence time scales [23].

These previous studies show consistently that S_T increases in the LTI regime, however, the underlying physics is unclear and requires further investigation. For example, the influence of the increased mixture temperature, the decreased Lewis number, and the change of composition due to LTI on S_T is not fully understood. A lower Lewis number tends to enhance the thermal-diffusive instability of the flame, which in turn could increase the burning velocity. An increase of the mixture temperature leads to a decrease of mixture density, which could on one hand increase the laminar burning velocity [24] and on the other hand suppress the hydrodynamic instability due to the decrease of density ratio between the burnt side and the unburnt side of the flame, which in turn could suppress the burning velocity. In a LTI reformer gas RCCI engine study, Geng et al. [19] reported that the mixture after LTI is less reactive than fresh fuel/air mixture, since the ignition of the mixture after LTI is retarded

and the heat release rate is slower than that in the fresh fuel/air mixture without LTI reforming gas. These results showed an opposite trend of LTI effect on the combustion process to that in the RATS burner experiments. These contradictory trends of LTI effects may be due to the relatively higher importance of the mixture temperature after LTI than that of mixture composition, since the LTI gas in Geng et al. [19] was kept a constant temperature by cooling the LTI gas down to its temperature before LTI, before being rerouted into the engine cylinder.

The above literature reviews indicate that the complex LTI/flame/flow interaction and its effect on burning velocity in LTI regime are not well understood. Note that in the CF flame regime no LTI reactions take place before the mixture reaching the premixed flame front, whereas in the LTI flame regime the LTI reactions commence not only inside the burner but also continue until the mixture reaching the flame front. This paper aims to address this issue and explore the behavior of LTI gas flames in the RATS burner [16]. The goals are (i) to investigate the impact of LTI reactions on the flame structures, and (ii) to identify the mechanisms that control of the propagation speed of the reaction front in different regimes. Three-dimensional (3D) large eddy simulation (LES) and two-dimensional detailed numerical simulation of laminar flames (2DLF) are carried out for different conditions, covering chemically frozen (CF) to LTI gas flames. The structures of flames in the CF and LTI regimes, and the transition regime from CF to LTI are analyzed. The effect of LTI chemistry and species transport (Lewis number) is analyzed to identify their impact on the flames.

2. Numerical method

The Favre-filtered conservation equations used in the LES can be written as:

$$\frac{\partial \bar{\rho}}{\partial t} + \frac{\partial \bar{\rho}\tilde{u}_\mathrm{j}}{\partial x_\mathrm{j}} = 0 \tag{1}$$

$$\frac{\partial \bar{\rho}\,\tilde{u}_\mathrm{i}}{\partial t} + \frac{\partial}{\partial x_\mathrm{j}}[\bar{\rho}\,\tilde{u}_\mathrm{i}\tilde{u}_\mathrm{j} - \bar{\tau}_\mathrm{ij} + \tau_\mathrm{ij}^\mathrm{sgs}] = 0 \tag{2}$$

where, tilde denotes the Favre filtering $\overline{\rho u} = \bar{\rho}\tilde{u}$. Overline denotes the spatial filtering, e.g., $\overline{u(x,t)} = \int G(r,x)u(x-r,t)dr$, where the integration is over the entire field and the filter function *G* satisfies the normalization condition:

$$\int G(r,x)dr = 1 \tag{3}$$

In Eq. 2, u is a velocity component and $\bar{\tau}_\mathrm{ij}$ is the filtered stress tensor, which can be expressed as $\bar{\tau}_\mathrm{ij} = -\bar{p}\delta_\mathrm{ij} + 2\mu(\tilde{S}_{ij} - 1/3\tilde{S}_{kk}\delta_\mathrm{ij})$, $\tau_\mathrm{ij}^\mathrm{sgs}$ is the sub-grid scale (SGS) stress tensor which is modeled using the dynamic Smagorinsky [25] turbulence model. Favre-filtered conservation equations for species and energy can be written as follows:

$$\frac{\partial(\bar{\rho}\tilde{Y}_\mathrm{k})}{\partial t} + \frac{\partial[\bar{\rho}(\tilde{u}_\mathrm{i}+\tilde{v}_\mathrm{ci})\tilde{Y}_\mathrm{k}]}{\partial x_\mathrm{i}} = \frac{\partial}{\partial x_\mathrm{i}}\left(\left(\frac{\mu_\mathrm{t}}{Sc_\mathrm{t}} + \bar{\rho}\overline{D_\mathrm{k}}\right)\frac{\partial \tilde{Y}_\mathrm{k}}{\partial x_\mathrm{i}}\right) + \bar{\dot{\omega}}_\mathrm{k} \tag{4}$$

$$\frac{\partial(\bar{\rho}\tilde{h}_\mathrm{s}+K)}{\partial \mathrm{t}} + \frac{\partial(\bar{\rho}\tilde{u}_\mathrm{i}\tilde{h}_\mathrm{s}+K)}{\partial x_\mathrm{i}} = \frac{\partial \bar{p}}{\partial t} + \frac{\partial}{\partial x_\mathrm{i}}\left(\left(\frac{\mu_\mathrm{t}}{Pr_\mathrm{t}} + \frac{\bar{\lambda}}{\bar{C}_\mathrm{p}}\right)\frac{\partial \tilde{h}_\mathrm{s}}{\partial x_\mathrm{i}}\right) + \nabla\cdot\left(\bar{\rho}\sum_\mathrm{i}^\mathrm{N}\tilde{h}_\mathrm{si}\tilde{J}_\mathrm{i}\right) + \bar{\dot{\omega}}_\mathrm{h} \tag{5}$$

where $\tilde{Y}_\mathrm{k}$, $\tilde{h}_\mathrm{s}$, *K*, $\overline{D_\mathrm{k}}$, $\bar{\lambda}$, $\bar{C}_\mathrm{p}$, denote the filtered mass fraction of species k, sensible enthalpy, turbulent kinetic energy, mass diffusivity of species k, thermal conductivity and heat capacity, respectively. Differential diffusion is considered, hence, $\overline{D_\mathrm{k}}$ is calculated from binary diffusion coefficient. $\tilde{v}_\mathrm{ci}$ is the correction velocity to ensure mass conservation. The third term in the right-hand side of Eq. 5 is the heat flux associated with species diffusion of different enthalpies. μ_t is turbulent viscosity, and

Sc_t and Pr_t are turbulent Schmidt number and turbulent Prandtl number. $\bar{\dot{\omega}}_k$ is the net rate of production (ROP) of species k, and $\bar{\dot{\omega}}_h$ is the total heat release rate (HRR). Finite rate chemistry with a well-stirred reactor (WSR) SGS model is employed here, and the extrapolation-algorithm seulex ordinary differential equation solver based on the linearly implicit Euler method [26] is used to solve the stiff chemistry system. Filtered equation of state for ideal gas is used to close the equation system.

The open source CFD platform, OpenFOAM 6 [27], is used to solve the governing equations for turbulent reacting flows. The finite volume method with third-order cubic scheme [28] is adopted for the spatial discretization and implicit second-order backward Euler scheme is used for the time integration. The detailed transport properties are calculated by the logarithm polynomial fitting method [29] and mixture-average model is adopted to calculate the mixture transport properties. For the 2DLF cases, the low Mach number reacting flow DNS code developed in OpenFOAM in the authors' group [30] is used. Previous results [31][32] have shown that the OpenFOAM code is capable for the detailed numerical simulation of premixed laminar flame when the detail transport properties are considered.

3. Simulation setups and parameters

The cases presented in this paper are based on the experiment of RATS burner of Won et al. [16]. This burner has been developed to investigate turbulent flame regimes for large hydrocarbon fuels exhibiting LTI behavior. Fig. 1 presents a schematic

diagram of RATS burner, an instantaneous isosurface of temperature in the 3D domain, and a local flame front along with the LES mesh, respectively. To minimize the computational time, the current simulation focuses on the computational domain downstream the burner exit. Consequently, the computational domain is a cuboid with a size of 60 mm × 92 mm × 92 mm. The fuel inlet is a rectangular channel with the length of 40 mm × 10 mm at the center of the domain bottom. A pilot flame burner with a dimension of 1 mm × 40 mm is placed on both sides of the fuel inlet. A refined regular hexahedron mesh with 156 μm size is adopted to cover the pilot and main flame regions as shown in Fig. 1c, resulting in a grid of 6.7 million cells. The top and the lateral boundaries are prescribed as pressure outlet conditions, and zero-gradient boundary condition is used for scalar variables. The maximal Courant number is set to 0.1 to ensure the numerical stability, which leads to a maximal time step about 1 μs

According to the RATS burner experiment [16], the vaporized n-heptane and air are mixed in a 61 cm flow reactor. By varying the heated flow residence time and reactant temperature, the premixed n-heptane/air mixture with different species are injected to the domain. A homogenous ignition process of the mixture in zero-dimension (0D) reactor module of Chemkin [33] is simulated to obtain the intermediate species under the same flow residence time. These species are taken as LES inlet conditions, which is acceptable since the species and temperature are fairly uniformly distributed at the exit of the RATS burner after long time mixing in the burner. The same inflow mixture conditions were also considered in [22].

The pilot flame was considered in the computation using a premixed gas inflow boundary condition with a constant mass flow rate. A homogenous turbulence field generated using the method of LEMOS [34] is superimposed on a power law velocity profile as the inlet velocity. The turbulence intensity is set as 12.5% of the bulk velocity [16], and the integral scale is 2.5 mm for all cases, i.e., 25% of the inlet channel width.

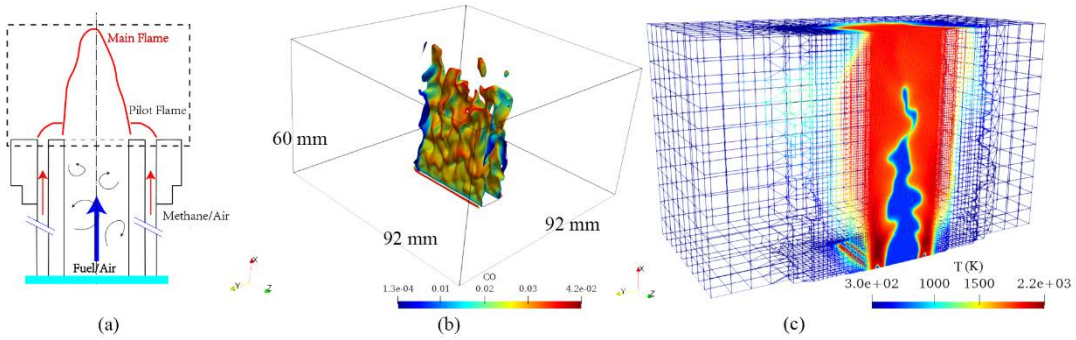

Figure 1. (a) A schematic diagram of RATS burner [16]. (b) Iso-surface of temperature (T= 1490 K) colored with CO mass fraction. (c) Local mesh refinement in the flame region.

The skeletal n-heptane mechanism from Lu et al. [35], including 68 species and 283 elementary reactions, is used in the present numerical simulations. A comparison between the skeletal and the detailed chemical mechanisms [36] for n-heptane/air mixture is made for the ignition delay time and S_L in Fig. 2. The detailed mechanism consists of 1550 species and 6000 reactions. It is found that the mechanism of Lu et al. yields satisfactory prediction of ignition delay time and laminar flame speed for the initial temperature ranging from 650 K to 700 K, covering the temperature range of the RATS burner experiment. The results from the skeletal mechanism are in fairly good

agreement with that from the detailed mechanism.

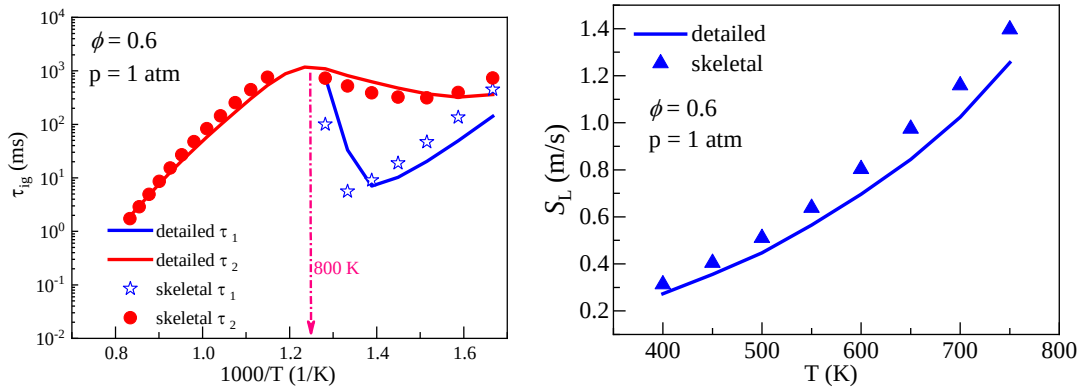

Figure 2. The comparison of ignition delay time (left) and S_L (right) for n-heptane/air mixture between skeletal (symbols) and detailed (lines) chemical mechanisms.

The initial conditions and case setups are described in Table 1. U_0 is the bulk flow velocity of fuel/air mixture, u' the root-mean square (RMS) of velocity fluctuation, ϕ the equivalence ratio of the fuel/air mixture and τ_r the residence time of the fuel/air mixture inside the burner, which is the time duration that the mixture undergoes LTI reactions before being injected to the computational domain. τ_1 is the time at which the onset of first stage ignition takes place in the mixture. T_0 is the initial temperature of the mixture, which is also the initial temperature of the reactant mixture in the pilot flame in the corresponding cases. T_u is the mixture temperature at the RATS burner exit. S_{L0} is the laminar burning velocity of the initial mixture (before the onset of LTI reactions) calculated with the Lu et al. mechanism and detailed transport properties. The combustion process is at atmospheric pressure, with an ambient air temperature of 300 K. In Table 1, U_p is the pilot burner flow speed. Since the mass flow rate of pilot

flame is kept constant for all cases investigated, the inlet velocity of the pilot burner varies with the initial temperature, e.g., 4 m/s at 600 K and 4.33 m/s at 650 K.

The effects of initial temperature and Lewis number on turbulent burning velocity are investigated for Cases 1-5 using LES, and for Cases 6-9 using 2DLF. In 2DLF, the mesh size is 20 μm, and about 20 cells are used to resolve the thermal flame thickness.

Table 1. Initial conditions for LES and 2DLF cases

	case	ϕ	U_0 (m/s)	u' (m/s)	U_p (m/s)	T_0 (K)	T_u (K)	τ_1 (ms)	τ_r/τ_1	Le	S_{L0} (m/s)	state
LES	1	0.6	10	1.25	4	600	600	488	0.13	≠1	0.80	CF
	2	0.6	10	1.25	4.33	650	669	65.60	0.97	≠1	0.97	Tran*
	3	0.6	10	1.25	4.67	700	837	14.39	4.43	≠1	1.16	LTI
	4	0.6	10	1.25	4	600	600	488	0.13	=1	0.80	CF
	5	0.6	10	1.25	4.67	700	837	14.39	4.43	=1	1.16	LTI
2DLF	6	0.6	10	0	4.5	700	700	14.39	0	1	1.16	CF
	7	0.6	10	0	4.5	700	837	14.39	4.43	1	1.16	LTI
	8	0.6	10	0	4.5	700	700	14.39	0	≠1	1.16	CF
	9	0.6	10	0	4..5	700	837	14.39	4.43	≠1	1.16	LTI

* Tran denotes the transition regime from the LTI regime to the CF regime.

4. Results and discussion

4.1 LES study

4.1.1 Comparison of LES results with experiments

Fig. 3 shows the photography of three flames (Cases 1-3) in the RATS burner experiment [16] and the corresponding LES time averaged temperature distribution. Well-defined flame cones can be identified in the photography and the mean temperature field. The cone angle is directly related to the burning velocity [31]. As the initial temperature of the reactants increases, the flame height decreases and the flame

cone angle increases, indicating an enhanced burning velocity, cf., Figs. 3a, b. In addition, for Case 3, the residence time (τ_r = 63.75 ms) is longer than its first-stage ignition delay time (τ_1 = 14.39 ms), therefore, LTI occurs and alters the composition and temperature of the mixture before being injected into the computational domain.

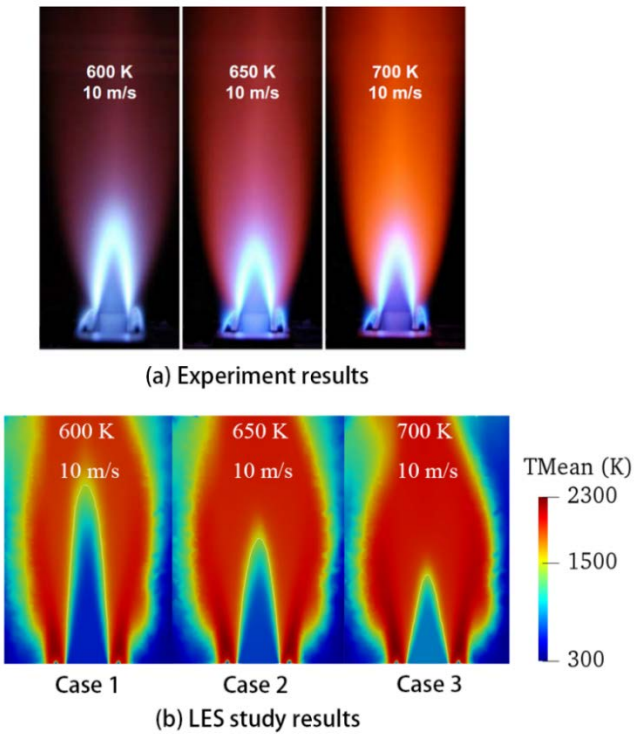

Figure 3. (a) Photography of n-heptane/air turbulent flames from the RATS burner experiment [16], (b) time averaged temperature distribution from LES.

To calculate the turbulent burning velocity (S_T), a flame front was identified based on a threshold value of OH fluorescence intensity in the experiment [16]. The turbulent burning velocity was calculated based on the time averaged OH PLIF images. In the LES, the flame front is defined at the location of the maximum gradient of OH mass fraction. S_T can be obtained from the mass flow conservation law,

$$S_{\mathrm{T}} = U_0 W / P_{\mathrm{avg}} \quad (6)$$

where W is the inlet width, and P_{avg} is the flame surface length. Fig. 4 compares the normalized turbulent burning velocity between LES (Cases 1-5) and experimental measurement, where in the experiments the mixture has a lower equivalence ratio. For conventional premixed flames (the CF regime), a higher turbulent intensity tends to yield a higher turbulent burning velocity [37]. However, this trend does not hold during the transition from the CF regime to the LTI regime, as indicated by the experimental data and LES data in Fig. 4. In the experiment [16], from CF to LTI regimes, and in the LES (Cases 1 to 3), $S_{\mathrm{T}}/S_{\mathrm{L0}}$ increases with increasing T_0, despite that the turbulence intensity (u'/S_{L0}) decreases. This indicates that the effect of LTI chemistry has a more profound impact on the turbulent burning velocity than the impact of flame/turbulence interaction.

Furthermore, by comparing the result of Case 3 with that of Case 5 and the results of Case 1 with that of Case 4, it is found that the influence of differential diffusion on the turbulent burning velocity is more significant in the LTI regime than in the CF regime. In the LTI regimes, $S_{\mathrm{T}}/S_{\mathrm{L0}}$ with the differential diffusion effect taken into account (non-unity Lewis number) is higher than the corresponding one without differential diffusion (unity Lewis number). This result is consistent with previous theoretical analysis that shows S_{T} being inversely proportional to the square root of Lewis number [21]. In the CF regime, however, an opposite trend is predicted in LES, even though the effect of differential diffusion plays a less significant role in CF regime

(see Case 1 and Case 4). This is consistent with the expectation that in turbulent flames the SGS transport effect is more important than the molecular transport, so that detailed transport properties may be neglected in LES [38]. The above effect of differential diffusion in the LTI and CF regimes needs to be further analyzed. To do this, a detailed investigation of chemistry-molecular transport interaction in the LTI regime is conducted for the 2DLF cases. The results will be presented in Section 4.2.

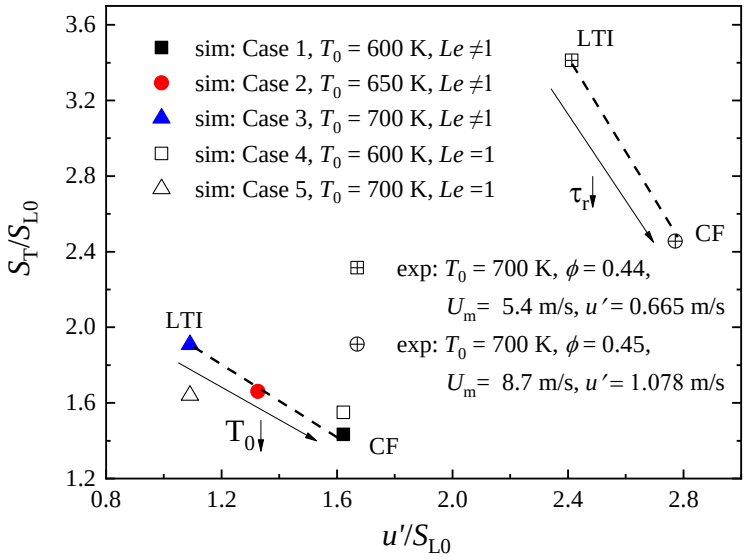

Figure 4. Normalized turbulent burning velocity for Cases 1-5 from LES and experiments under similar initial temperature but different equivalence ratio conditions [16].

4.1.2 Flame structures in different regimes

Fig. 5 presents the 2D instantaneous distribution of temperature, mass fraction of n-heptane (NC_7H_{16}), CH_2O, OH and CO for Cases 1-3, covering three flame regimes, CF, transition from CF to LTI, and LTI regimes, with T_0 varying from 600 to 700 K, respectively. In Case 1, CH_2O appears in a thin layer, separating the n-heptane/air

region upstream and the OH radical region downstream. Case 1 shows thus a conventional premixed flame structure. The CO layer is rather thin, indicating that CO oxidation occurs rapidly in the flame in the present fuel-lean combustion condition (ϕ = 0.6). By increasing the initial temperature from 600 K to 650 K, Case 2 shows a thin CH_2O layer in the near burner region and a broad CH_2O layer in the tip of the flame. Upstream the CH_2O layer the fuel (n-heptane) is shown to be oxidized in a broad region. The fuel oxidation is by virtue of LTI reactions, in which the level of OH radical is low, and the temperature increase in this LTI process is not significant. In the LTI reactions, large hydrocarbon species are firstly decomposed to small hydrocarbon species, such as CH_2O [9][39], which is thus an important intermediate in the low-temperature oxidation of n–heptane and may be identified as a LTI reaction marker. The structures of the OH and CO layers downstream the CH_2O layer are similar to those in the CF regime, Case 1.

Further increase of the initial temperature to 700 K in Case 3, the LTI reactions take place already inside the burner. Rather homogenous distribution of CH_2O can be found in the entire region upstream the OH layer. In this region, certain low concentrations of fuel and CO can be observed. This result is consistent with the previous finding that the $CH_2O \rightarrow HCO \rightarrow CO$ is one of the reaction pathways in LTI [9]. Comparing the three cases, it is found that the extent of flame wrinkling decreases from CF regime to LTI regime, along with a decreasing flame height, indicating an increasing burning velocity but a decreasing effect of turbulent flame wrinkling.

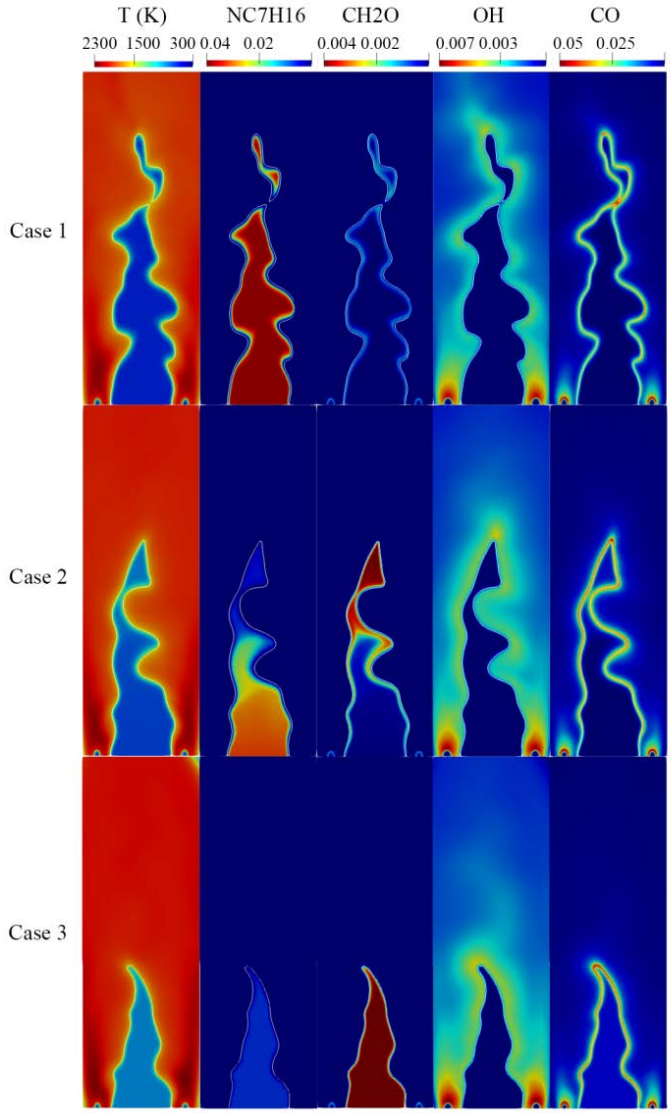

Figure 5. The instantaneous distributions of temperature, mass fraction of NC_7H_{16}, CH_2O, CO and OH (from left to right column) in Cases 1-3 (CF, transition from CF to LTI, and LTI regimes), respectively.

4.2 Two-dimensional laminar flame studies

In the LTI regime, the increased S_T is a result of species transport, chemical kinetics and turbulence/flame interaction [21]. Recent DNS [22] showed that the increment of S_T could be attributed to the increase of laminar burning velocity when the

flame is varied from the CF regime to the LTI regime at constant Karlovitz number. In order to gain further insight into this problem, we carried out a series of 2DLF cases to discriminate the effect of LTI (Cases 6, 7) and detailed transport properties (Cases 8, 9) on the burning velocity by neglecting the effect of turbulence. The case setups and initial conditions have been shown in Table 1, covering the CF and the LTI regimes.

4.2.1 Heat release region and chemical reaction path

Fig. 6 shows the CH_2O mass fraction distribution for Cases 6-9. It is clear that in both the CF and the LTI regimes, considering differential diffusion leads to a higher S_{L1} especially for the LTI regime. Note that, for consistency, the values of S_{L1} in Fig. 6 are calculated using the same method used in LES study. S_{L1} is different from S_{L0} in that the former is the laminar burning velocity of a slot burner with the inflow mixture undergone LTI reactions, whereas the latter is the laminar burning velocity of unstretched flame with an initial mixture without LTI reactions. As will be shown later (in Sec. 4.2.2), the diffusion of low Lewis number species, e.g., H_2, from the burnt side to unburnt side is higher in the case with differential diffusion than that in the unity Lewis number case, which gives rise to a change of flame structure under the current fuel-lean conditions ($\phi = 0.6$).

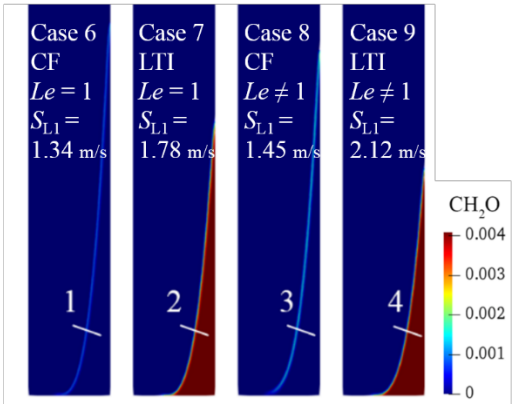

Figure 6. CH_2O mass fraction distribution of 2DLF for Cases 6-9.

Chemical reaction path analysis is performed to study the effects of LTI chemistry and transport properties. Fig. 7 shows the HRR distribution along Line 1 (CF, *Le* = 1), Line 2 (LTI, *Le* = 1), Line 3 (CF, *Le* ≠ 1) and Line 4 (LTI, *Le* ≠ 1) for Cases 6-9, respectively. The flame coordinate in Fig. 7 (as well as in Figs. 8 and 9 to be shown later) has been shifted to have x = 0 at the peak HRR, with x << 0 being the preheat zone while x >> 0 the post flame zone. It is seen that Line 1 (Case 6) in CF regime has the highest peak HRR in the flame front. Line 4 (Case 9) in the LTI regime shows the broadest HRR region, indicating a change of species reactivity from the CF regime to the LTI regime. In both regimes, considering the differential diffusion leads to a broadened HRR region due to the difference in the diffusion rate of species across the flame.

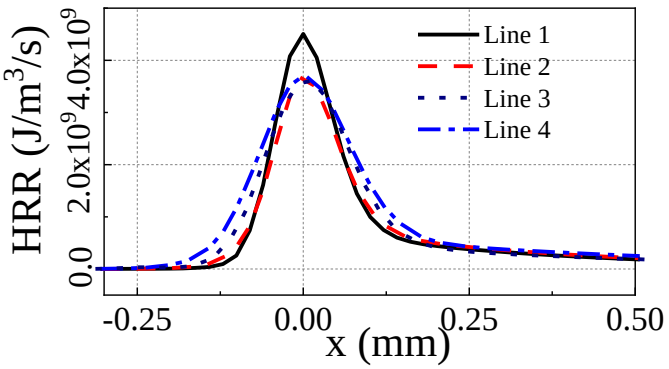

Figure 7. HRR distribution along Line 1 (CF, *Le* = 1), Line 2 (LTI, *Le* = 1), Line 3 (CF, *Le* ≠ 1) and Line 4 (LTI, *Le* ≠ 1). The line numbers are indicated in Fig 6.

In order to understand the detailed chemical reaction pathway, seven key elementary reactions that contribute the most to the heat release rate are identified, as shown in Table 2. Three of these reactions form the carbon flow reaction pathway, $CH_2O \xrightarrow{R7} HCO \xrightarrow{R2} CO \xrightarrow{R5} CO_2$. Spatial distribution of HRR from reactions R2, R3, R5 and R7 for the CF case (Lines 1, 3) and the LTI case (Lines 2, 4) are shown in Fig. 8. It is clear that these four reactions are intensified in the LTI regime (Line 4), as compared with that in the CF regime (Line 3), due to the higher amount aldehyde (e.g., CH_2O) produced in the LTI reaction far upstream. Among these reactions, R2, R3 and R7 contribute more to the heat release in the inner layer of the reaction zone towards the preheat zone and R5 shows a wider heat release region in the CO oxidation layer. These elementary reactions are significantly enhanced by differential diffusion in LTI regime, as shown in Fig. 8. Comparatively, for the CF flames, the differential diffusion effect is less significant. The above elementary reactions involve radicals such as H, O, and OH. The important differential diffusion effect in the LTI regime is attributed to variation of

these radicals in the reaction zone, as analyzed below.

Table 2. Top seven exothermic elementary reactions contributing the most to HRR

Name	Elementary reaction
R1	$CH_3+O \Leftrightarrow CH_2O+H$
R2	$HCO+O_2 \Leftrightarrow CO+HO_2$
R3	$HO_2+OH \Leftrightarrow H_2O+O_2$
R4	$CH_2(S)+O_2 \Leftrightarrow CO+OH+H$
R5	$CO+OH \Leftrightarrow CO_2+H$
R6	$HCO+OH \Leftrightarrow CO+H_2O$
R7	$CH_2O+OH \Leftrightarrow HCO+H_2O$

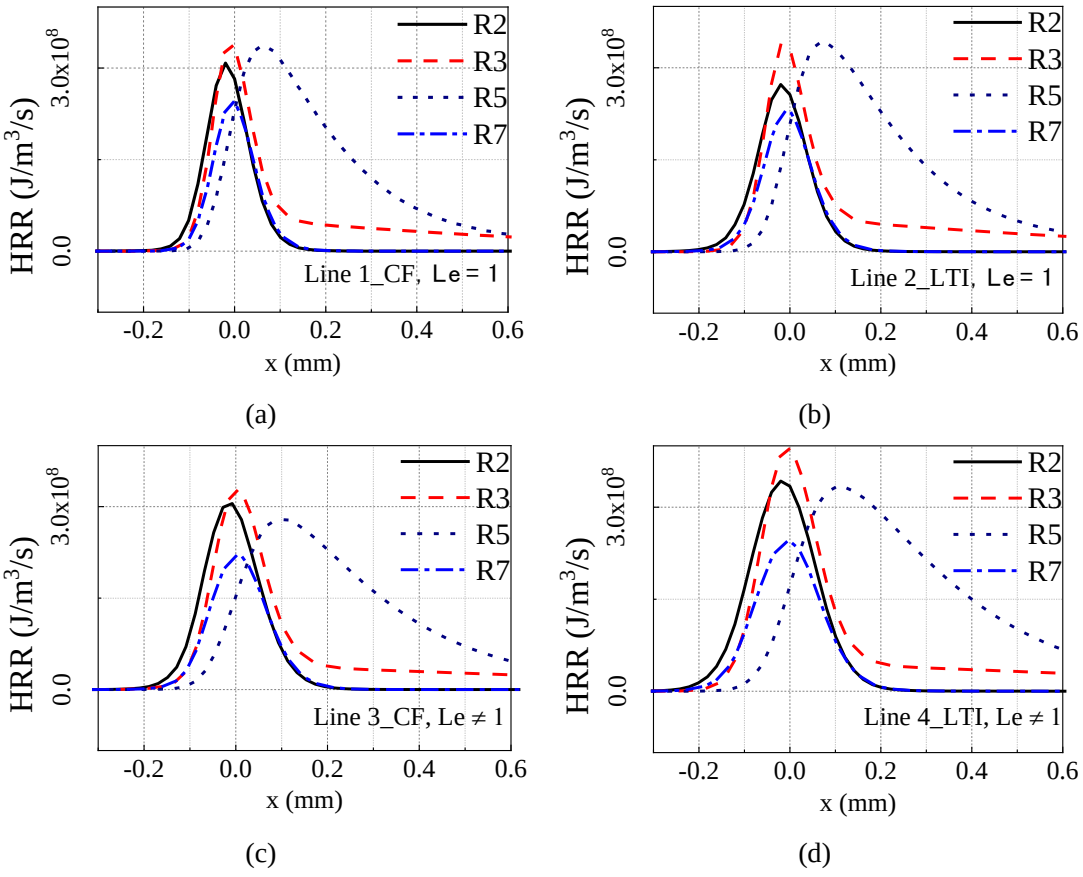

Figure 8. Spatial distribution of HRR from key elementary reactions for Cases 6-9, along the reaction path $CH_2O \rightarrow HCO \rightarrow CO \rightarrow CO_2$.

4.2.2 Transport budget term analysis

As shown above, some key elementary reactions, e.g., R2 and R3, are intensified in the LTI regime. Fig. 9 show the mass fraction and ROP profiles of CH_2O,

OH, H_2, and H radicals across the flame along Lines 2, 3, and 4. Consistent with the HRR profiles, the peak consumption rate of CH_2O is increased by a factor of two in the LTI regime (Line 4) as compared with that in the CF regime (Line 3). However, the ROPs of OH and H, and the OH and H profiles are similar to their counterpart in the two regimes, indicating that the reactivity of high temperature reactions is not affected. This result is consistent with the previous study [22] that the preheat zones in the CF and the LTI regimes show considerable differences (e.g., with higher CH_2O and H_2), while reaction zones remains qualitatively similar.

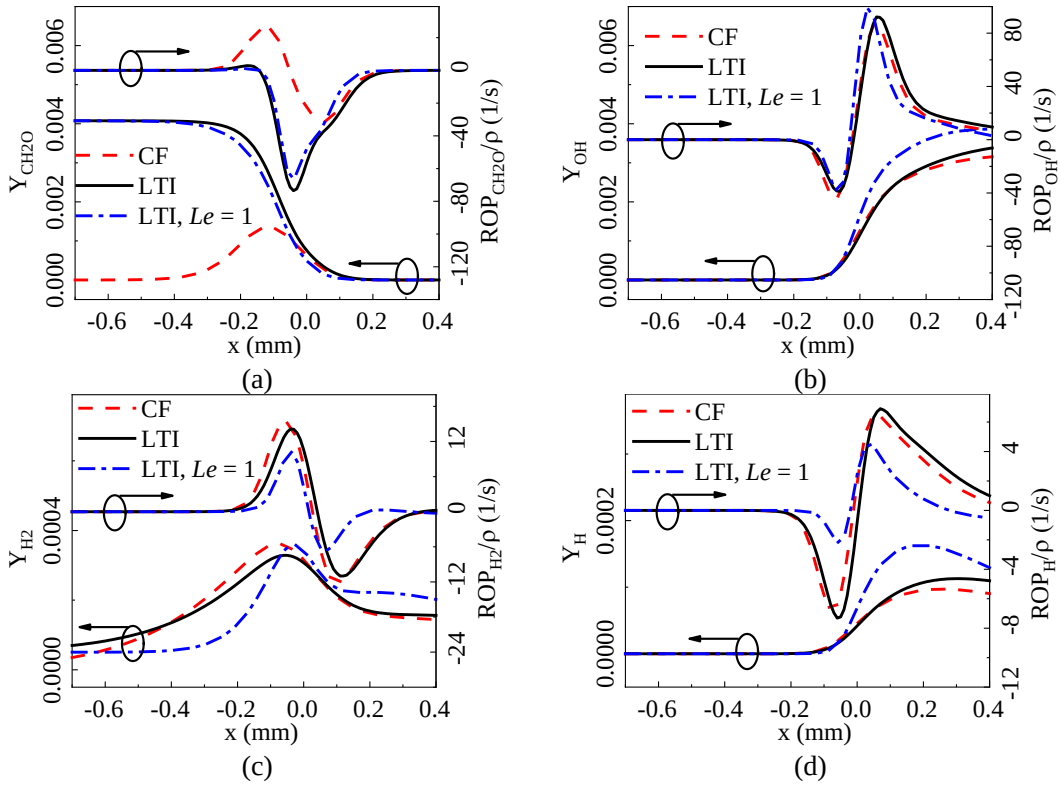

Figure 9. Species mass fractions and ROPs of CH_2O (a), OH (b), H_2 (c) and H radicals (d) along Line 2 (LTI, *Le* = 1), Line 3 (CF) and Line 4 (LTI).

The effect of differential diffusion can be identified when comparing the LTI cases with and without differential diffusion. When Le = 1 is assumed, the diffusion of H_2 from the reaction zone to the preheat zone is significantly slower. Subsequently, the mass fraction of H_2 in the preheat zone is significantly lower. Due to the lower diffusion rate of H radicals in the Le = 1 case, the mass fraction of H radicals in the radical formation zone (as indicated by the peak of ROP of H radicals) is higher, although the value of the ROP peak of H radicals is lower than that in the case with $Le \neq 1$. Due to slower diffusion of H radicals to the inner layer, the consumption rate of H radicals (i.e., negative ROP of H radicals) is lower in the Le = 1 case, along with slower heat release rate in the inner layer. This explains the significant enhancement of key elementary reactions R2, R3 and R7 by differential diffusion in LTI regime.

A question is that if the reactivity of some intermediate species is enhanced in the LTI regime, how will the overall reactivity of unburnt mixture changes subsequently? To address this question, the flame displacement speed S_d is analyzed based on oxygen molecular mass fraction, Y_{O2}, as follows:

$$S_d = -\frac{\nabla\cdot(\rho D_{O2}\nabla Y_{O2})+ROP_{O2}}{\rho|\nabla Y_{O2}|} \quad (7)$$

$$S_{L2} = \frac{\rho S_d}{\rho_u} = -\frac{\nabla\cdot(\rho D_{O2}\nabla Y_{O2})/\rho_u+ROP_{O2}/\rho_u}{|\nabla Y_{O2}|} \quad (8)$$

where S_d is the local displacement of an iso-contour of Y_{O2} in any locations across the flame, whereas S_{L2} is the local displacement speed of the iso-contour of Y_{O2} on the unburnt side of the flame. D_{O2}, ROP_{O2}, ρ and ρ_u denote the mass diffusion coefficient of oxygen, the ROP of oxygen, the local density of the mixture and the density of the

unburned mixture.

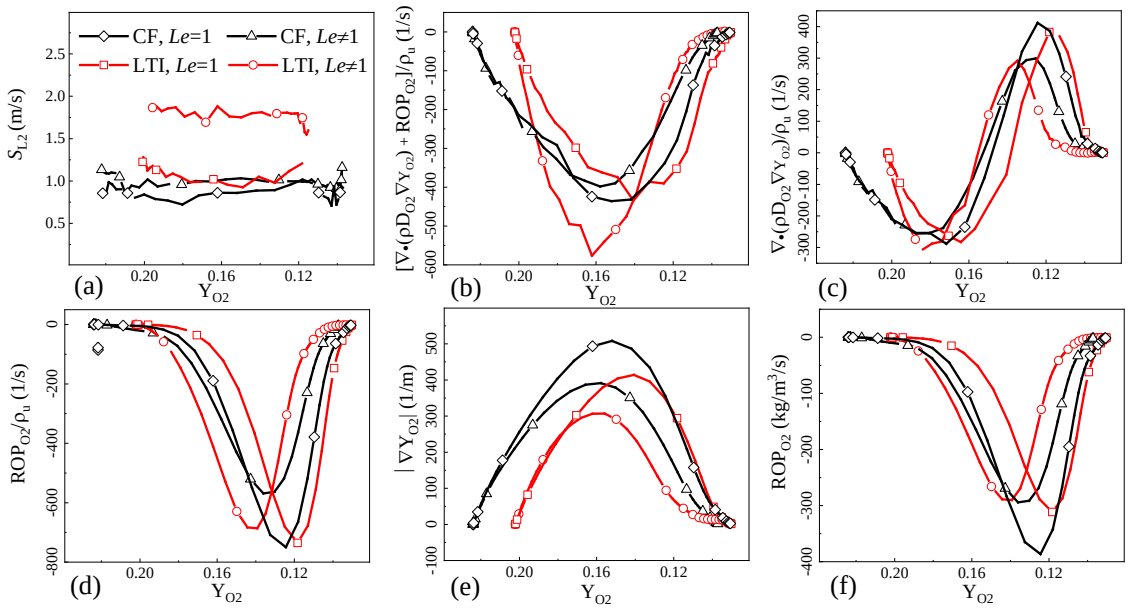

Figure 10. S_{L2} (a), the budget terms of S_{L2} (b, c, d), $|\nabla Y_{O2}|$ (e) and ROP_{O2} (f) as a function of Y_{O2} along Lines 1 (CF, Le = 1), 2 (LTI, Le = 1), 3 (CF, $Le \neq 1$) and 4 (LTI, $Le \neq 1$). The unburnt mixture density (ρ_u) in LTI case is 0.423 kg/m^3 and in CF case is 0.517 kg/m^3.

Fig. 10 displays the values of S_{L2}, the budget terms of Eq. 8, and the gradient of Y_{O2}, ∇Y_{O2}, as a function of Y_{O2} across the flame fronts for the CF (along Lines 1, 3) and the LTI (along Lines 2, 4) cases. S_{L2} is nearly a constant when evaluated at different flame locations in each flame case (iso-contour values of Y_{O2}), indicating that the flow is steady and quasi one-dimensional (1D) across the flame fronts. It is shown that S_{L2} in the LTI regime is a factor of 1.75 of that in CF regime when differential diffusion is taken into account (non-unity Lewis number), cf., Line 3 and Line 4, whereas without differential diffusion (unity Lewis number), S_{L2} in the LTI regime is only slightly higher

than that in the CF regime, cf. Line 1 and Line 3. This result is consistent with that of S_{L1} shown in Fig. 6, although they are representing two different physical quantities, with S_{L1} denoting the overall flame speed while S_{L2} being the local displacement speed at the flame positions as indicated in Lines 1-4 in Fig. 6.

Consistent with the HRR profiles shown in Fig. 7, the highest oxygen consumption rate (ROP_{O2}) is along Line 1, i.e., in the CF flame case with unity Lewis number, cf. Fig. 10f. In the LTI flame case with non-unity Lewis number, the oxygen consumption is shifted towards the preheat zone (towards higher Y_{O2} side). According to Eq. 8, the budget ROP term contribution to S_{L2} is the oxygen consumption rate normalized by the unburned reactant density, ROP_{O2}/ρ_u. Due to the lower value of ρ_u in the LTI flames, the peak values of ROP_{O2}/ρ_u in the LTI flames is nearly the same as that in the CF flame with unity Lewis number. The LTI flame with non-unity Lewis number has, however, a significantly higher value of ROP_{O2}/ρ_u towards the preheat zone.

The peak values of the normalized oxygen diffusion rate, $\nabla \cdot (\rho D_{O2} \nabla Y_{O2})/\rho_u$, are similar in the CF and LTI flame cases; however, the peaks of the normalized diffusion rate are shifting towards the preheat zone in the non-unity Lewis number cases. The net effect of shifting the diffusion rate towards the preheat zone when the differential diffusion is taken into account and the enhanced ROP towards the preheat zone in the LTI cases leads to a significantly high peak value of the budget terms $[\nabla \cdot (\rho D_{O2} \nabla Y_{O2}) + ROP_{O2}]/\rho_u$ for the non-unity Lewis number LTI case, cf. Fig. 10b. This

is the main mechanism behind that the LTI flame has the highest value of S_{L2}, Fig. 10a.

According to Eq. 8, the value S_{L2} is inversely proportional to ∇Y_{O2}. Due to the LTI reactions, the value of Y_{O2} in unburned reactant mixture of the LTI cases is lower than that in the CF cases. The net effect of the lower Y_{O2} in the unburned reactant mixture and the broadened reaction zone leads to a significantly lower value of ∇Y_{O2} in the LTI flames, Fig. 10e. Differential diffusion gives rise to further lower peak values of ∇Y_{O2}, due to the enhanced diffusion rate towards the preheat zone. This is another important mechanism behind the significantly higher value of S_{L2} in the non-unity Lewis number LTI flame, Fig. 10a.

4.2.3 Effect of LTI composition and temperature on flame propagation

The effect of temperature and composition of LTI gas on the burning velocity is evaluated by comparing the laminar burning velocities of neat n-heptane/air mixture (corresponding to the CF regime discussed earlier) and the same n-heptane/air mixture but after 63.75 ms ($4.43\tau_1$, Table 1) LTI reactions (hereafter referred to as the LTI gas mixture). The laminar burning velocity, denoted here as S_{L3}, is calculated for one-dimensional freely propagating flames using the n-heptane mechanism from Lu et al. [35] and detailed transport properties (the same as the 2D and 3D calculations discussed in the earlier sections). Fig. 11 shows two classes of flame conditions under the pressure and equivalence ratio conditions the same as that of Cases 8 and 9 in Table 1. The first

class starts from the conditions of Case 8 (marked as #1 in Fig.11) and ends at condition #4 (with initial temperature 837K), during which the initial temperature of the neat n-heptane/air mixture is continuously increased. The second class starts from the condition of Case 9 (with the initial temperature of the LTI gas of 837K, marked as #2), and ends at condition #3, which has the same LTI gas composition as that at condition #2 but at a lower temperature. It appears that S_{L3} increases with the initial temperature for both the neat n-heptane/air mixture and the LTI gas mixture. The sensitivity of S_{L3} to temperature (dS_{L3}/dT) is nearly identical for the two mixtures.

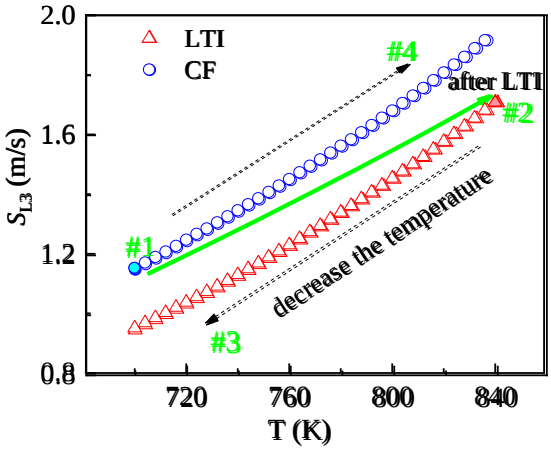

Figure 11. S_{L3} under different unburnt side temperatures in the CF and LTI regimes, with equivalence ratio of 0.6.

It is noteworthy to compare the two flame conditions, #1 (Case 8) and #2 (Case 9), Fig. 11. The initial fuel/air mixture is the same for the two flame conditions, while the only difference in the two mixtures is that in Case 9 (#2) the fuel/air mixture has undergone 63.75 ms LTI reactions. The sum of the thermal and chemical energy is the

same in the two flame conditions. With a lower chemical energy but a higher thermal energy, the LTI flame under condition #2 has a significantly higher burning velocity than the flame under condition #1. This result is consistent with the result discussed earlier in Section 4.2.2. However, if the temperatures of the neat n-heptane/air mixture and the LTI gas mixture are kept the same, the value of S_{L3} of the LTI gas is always lower than that of the corresponding neat n-heptane/air mixture. The existence of intermediate species such as CH_2O in the LTI gas reduces the reactivity of the mixture, since the chemical energy in the LTI gas is lower than that in the neat n-heptane/air mixture. This is consistent with LTI reformer gas RCCI engine experimental results of Geng et al. [19], which reported that the mixture after LTI is less reactive than fresh fuel/air mixture, with the ignition of the mixture after LTI retarded and the heat release rate slower than that in the fresh fuel/air mixture without LTI reforming gas.

5. Conclusions

Large eddy simulation is used to study turbulent premixed n-heptane/air flames in a pilot flame stabilized reactor assisted turbulent slot (RATS) burner under different flame regimes, including chemically frozen (CF) regime, and low temperature ignition (LTI) regime, and the transition regime from CF to LTI. In the LTI regime the low temperature reactions in the reactant upstream the flames give rise to a significant enhancement of turbulent burning velocity. The turbulent burning velocity in the LTI regime is found to be more sensitive to differential diffusion than that in the

conventional CF regime.

To understand the effects of LTI reactions and differential diffusion on the structures and propagation of the flames, a series of two-dimensional and one-dimensional laminar flames are simulated. It is found that owing to more diffusive reactants in the preheat zone due to LTI reactions, the heat release zone in the LTI regime is broadened. Consistent with the results of the turbulent flames in the RATS burner, differential diffusion shows a significant enhancement on the laminar burning velocity in the LTI regime, and a weaker effect in the CF regime. The fundamental mechanism behind is that differential diffusion can give rise to enhanced diffusion of reactive species such as H and H_2 between the high temperature reaction zones and the preheat zone, which enhances the rate of production towards the preheat zone. The enhanced laminar burning velocity in the LTI regime is a net effect of enhanced reaction and diffusion towards the preheat zone and the lower gradient of the reactant mass fraction (e.g., oxygen). These results imply that differential diffusion should be taken into account in combustion models for LTI flame propagation under low-to-medium turbulent intensity.

CRediT authorship contribution statement

Shenghui Zhong: Investigation, Visualization, Writing-Original draft preparation. **Fan Zhang:** Conceptualization, Writing-Reviewing and Editing. **Mehdi Jangi:** Methodology, Software, Data Curation. **Xue-Song Bai:** Formal analysis, Writing-Reviewing and Editing. **Mingfa Yao:** Resource, Project administration. **Zhijun Peng:** Funding acquisition, Supervision

Declaration of Competing Interest

The authors declare that they have no known competing financial interests or personal relationships that could have appeared to influence the work reported in this paper.

Acknowledgments

SZ gratefully acknowledge the financial support from the China Scholarship Council. This work was supported by National Natural Science Foundation of China No. 51876139 and 91541205. We thank Dr. Christopher B. Reuter from Princeton University for the valuable discussion and providing the experimental data. All the simulation cases are performed on TianHe-HPC1 system at National Supercomputer Center in Tianjin, China.

References

[1] Kalghatgi G. Is it really the end of internal combustion engines and petroleum in transport? Appl Energy 2018;225:965–74.

[2] Xu L, Bai X-S, Jia M, Qian Y, Qiao X, Lu X. Experimental and modeling study of liquid fuel injection and combustion in diesel engines with a common rail injection system. Appl Energy 2018;230:287–304.

[3] Li Y, Jia M, Liu Y, Xie M. Numerical study on the combustion and emission characteristics of a methanol/diesel reactivity controlled compression ignition (RCCI) engine. Appl Energy 2013;106:184–97.

[4] An Y, Raman V, Tang Q, Shi H, Sim J, Chang J, et al. Combustion stability study of partially premixed combustion with low-octane fuel at low engine load conditions. Appl Energy 2019;235:56–67.

[5] Xu L, Bai X-S, Li C, Tunestål P, Tunér M, Lu X. Combustion characteristics of gasoline DICI engine in the transition from HCCI to PPC: Experiment and numerical analysis. Energy 2019;185:922–37.

[6] Zhong W, Pachiannan T, Li Z, Qian Y, Zhang Y, Wang Q, et al. Combustion and emission characteristics of gasoline/hydrogenated catalytic biodiesel blends in gasoline compression ignition engines under different loads of double injection strategies. Appl Energy 2019;251:113296.

[7] Zhao W, Li Z, Huang G, Zhang Y, Qian Y, Lu X. Experimental investigation of direct injection dual fuel of n-butanol and biodiesel on Intelligent Charge Compression Ignition (ICCI) Combustion mode. Appl Energy 2020;266:114884.

[8] Pachiannan T, Zhong W, Rajkumar S, He Z, Leng X, Wang Q. A literature review of fuel effects on performance and emission characteristics of low-temperature combustion strategies. Appl Energy 2019;251:113380.

[9] Ju Y, Reuter CB, Yehia OR, Farouk TI, Won SH. Dynamics of cool flames. Prog Energy Combust Sci 2019;75:100787.

[10] Shi Z, Lee C, Wu H, Wu Y, Zhang L, Liu F. Optical diagnostics of low-temperature ignition and combustion characteristics of diesel/kerosene blends

under cold-start conditions. Appl Energy 2019;251:113307.

[11] Liu F, Shi Z, Zhang Z, Li Y, Sun C. Numerical study on critical ambient temperature for auto-ignition of the diesel spray under cold-start conditions. Fuel 2019;258:116191.

[12] Reuter CB, Lee M, Won SH, Ju Y. Study of the low-temperature reactivity of large n-alkanes through cool diffusion flame extinction. Combust Flame 2017;179:23–32.

[13] Zhang W, Faqih M, Gou X, Chen Z. Numerical study on the transient evolution of a premixed cool flame. Combust Flame 2018;187:129–36.

[14] Ju Y, Sun W. Plasma assisted combustion: Dynamics and chemistry. Prog Energy Combust Sci 2015;48:21–83.

[15] Pan J, Wei H, Shu G, Chen Z, Zhao P. The role of low temperature chemistry in combustion mode development under elevated pressures. Combust Flame 2016;174:179–93.

[16] Won SH, Windom B, Jiang B, Ju Y. The role of low temperature fuel chemistry on turbulent flame propagation. Combust Flame 2014;161:475–83.

[17] Skeen SA, Manin J, Pickett LM. Simultaneous formaldehyde PLIF and high-speed schlieren imaging for ignition visualization in high-pressure spray flames. Proc Combust Inst 2015;35:3167–74.

[18] Wang Y, Wei L, Yao M. A theoretical investigation of the effects of the low-temperature reforming products on the combustion of n-heptane in an HCCI

engine and a constant volume vessel. Appl Energy 2016;181:132–9.

[19] Geng C, Liu H, Cui Y, Yang Z, Fang X, Feng L, et al. Study on single-fuel reactivity controlled compression ignition combustion through low temperature reforming. Combust Flame 2019;199:429–40.

[20] Ju Y. Recent progress and challenges in fundamental combustion research. Adv Mech 2014;44:201402.

[21] Windom B, Won SH, Reuter CB, Jiang B, Ju Y, Hammack S, et al. Study of ignition chemistry on turbulent premixed flames of n-heptane/air by using a reactor assisted turbulent slot burner. Combust Flame 2016;169:19–29.

[22] Savard B, Wang H, Teodorczyk A, Hawkes ER. Low-temperature chemistry in n-heptane/air premixed turbulent flames. Combust Flame 2018;196:71–84.

[23] Krisman A, Hawkes ER, Chen JH. The structure and propagation of laminar flames under autoignitive conditions. Combust Flame 2018;188:399–411.

[24] Yu S, Bai X-S, Zhou B, Wang Z, Li ZS, Aldén M. Numerical Studies of the Pilot Flame Effect on a Piloted Jet Flame. Combust Sci Technol 2019:1–14.

[25] Lilly DK. A proposed modification of the Germano subgrid-scale closure method. Phys Fluids A Fluid Dyn 1992;4:633–5.

[26] Imren A, Haworth DC. On the merits of extrapolation-based stiff ODE solvers for combustion CFD. Combust Flame 2016;174:1–15.

[27] Jasak H, Jemcov A, Tukovic Z, others. OpenFOAM: A C++ library for complex physics simulations. Int. Work. coupled methods Numer. Dyn., vol.

1000, 2007, p. 1–20.

[28] Zirwes T, Zhang F, Habisreuther P, Hansinger M, Bockhorn H, Pfitzner M, et al. Quasi-DNS Dataset of a Piloted Flame with Inhomogeneous Inlet Conditions. Flow, Turbul Combust 2019:1–31.

[29] Kee RJ, Dixon-Lewis G, Warnatz J, Coltrin ME, Miller JA. A Fortran computer code package for the evaluation of gas-phase multicomponent transport properties. Sandia Natl Lab Rep SAND86-8246 1986;13:80401–1887.

[30] Zhong S, Zhang F, Peng Z, Bai F, Du Q. Roles of CO2 and H2O in premixed turbulent oxy-fuel combustion. Fuel 2018;234:1044–54.

[31] Hu S, Gao J, Gong C, Zhou Y, Bai XS, Li ZS, et al. Assessment of uncertainties of laminar flame speed of premixed flames as determined using a Bunsen burner at varying pressures. Appl Energy 2018;227:149–58.

[32] Yang Q, Zhao P, Ge H. reactingFoam-SCI: An Open Source CFD Platform for Reacting Flow Simulation. Comput Fluids 2019.

[33] Kee RJ, Rupley FM, Miller JA. Chemkin-II: A Fortran chemical kinetics package for the analysis of gas-phase chemical kinetics. 1989.

[34] Kröger H, Kornev N. Generation of divergence free synthetic inflow turbulence with arbitrary anisotropy. Comput Fluids 2018;165:78–88.

[35] Lu T, Law CK, Yoo CS, Chen JH. Dynamic stiffness removal for direct numerical simulations. Combust Flame 2009;156:1542–51.

[36] Mehl M, Pitz WJ, Westbrook CK, Curran HJ. Kinetic modeling of gasoline

surrogate components and mixtures under engine conditions. Proc Combust Inst 2011;33:193–200.

[37] Peters N. Turbulent combustion 2001.

[38] Lapointe S, Savard B, Blanquart G. Differential diffusion effects, distributed burning, and local extinctions in high Karlovitz premixed flames. Combust Flame 2015;162:3341–55.

[39] Splitter DA, Hanson RM, Reitz RD, Manente V, Johansson B, others. Modeling charge preparation and combustion in diesel fuel, ethanol, and dual-fuel PCCI engines. At Sprays 2011;21.